

GT2011-4) ) ( )

## EXPERIMENTAL INVESTIGATION OF LUBRICATION OIL FILM DYNAMICS IN A TYPICAL AERO-ENGINE BEARING CHAMBER ENVIRONMENT

Amir A. Hashmi, Klaus Dullenkopf,  
Hans-Jörg Bauer

Institut für Thermische Strömungsmaschinen  
(ITS), Karlsruhe Institute of Technology (KIT)  
76128 Karlsruhe, Germany  
Email: amir.hashmi@kit.edu

Michael Klingsporn

Air and Oil System,  
Rolls-Royce Deutschland Ltd & Co KG  
Eschenweg 11, Dahlewitz  
15827 Blankenfelde-Mahlow, Germany

### ABSTRACT

This paper deals with the wall film dynamics of lubrication oil in the vicinity of the scavenge port of a typical aero engine bearing chamber. Based on the major driving forces influencing the film dynamics, shear forces and gravity, two film flow regimes namely co & counter-current can be identified. The film flow in the bearing chambers is influenced by several factors which results in an undeveloped film thus making a comprehensive analysis of the flow field extremely difficult. A profound knowledge of the individual factors is required before a superposition can be performed. A simple test rig was designed and built to isolate and investigate the influence of major factors affecting the wall film dynamics in a typical bearing chamber environment. For the quantitative analysis, a parameter determined from the single phase pressure drop measurements (only in gas) is introduced to effectively analyze the undeveloped multiphase flow regime. It is shown that the momentum losses occurring in the counter-current regime become considerably greater than in the co-current regime when the shearing gas flow rate is increased beyond a certain value. For high gas flow rates (high shaft speeds in engine) the losses on the counter-current side (churning losses) can be several magnitudes larger than on the co-current side (no churning losses). It is also shown that for the conditions investigated and relevant to the bearing chamber, the possibility of waveforms leading to the droplet shedding on the co-current side is very unlikely. Significant droplet shedding occurs in the counter-current regime. Based on the results obtained, the possible characteristics of the near scavenge oil film in the absence of coexisting phenomena e.g. droplet interaction, off-take disturbances etc are outlined.

### INTRODUCTION

In Figure 1, the cross sectional view of the Institut für Thermische Strömungsmaschinen (ITS) high speed rotating bearing chamber is shown. The test rig represents a model bearing chamber where real engine conditions for high as well as intermediate pressure bearing chambers can be simulated [1]. In the last two decades, the test rig was intensively used e.g. [1, 2, 3, 4, 5, 6, 7, 8] with a large number of parameter variation studies to understand the two-phase flow phenomena in real aero engine bearing chambers.

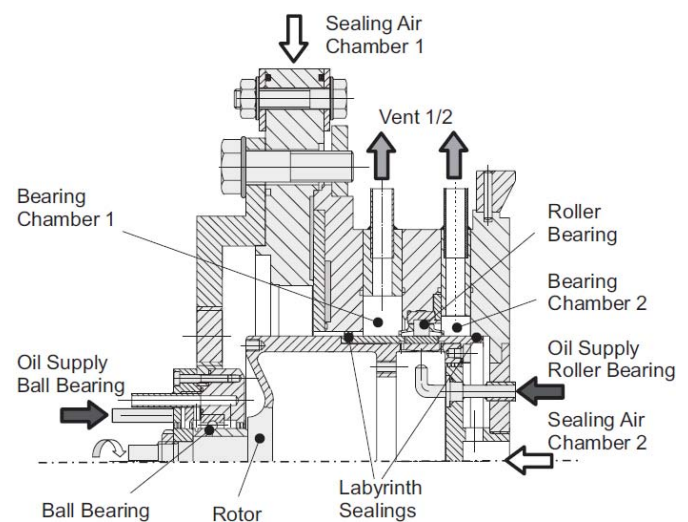


Figure 1. ITS high speed (model) bearing chamber test rig

In a high pressure bearing chamber, shaft speeds of 10000 - 15000 rpm occurs whereas a typical intermediate pressure bearing chamber observes 5000 – 7000 rpm during the engine operation. To avoid oil leakage, the labyrinth seals of the rig are pressurized with sealing air as in the real engine bearing chambers. The fast rotating shaft accelerates the air to almost 30% of the shaft tangential velocity [2]. Assuming a general case where the shaft rotates with 10000 (6000) rpm and a typical diameter of Ø100 mm then a mean air velocity of approx. 15 m/s (10 m/s) results in the high (intermediate) pressure bearing chamber. On the other hand, the oil film observed in the model bearing chamber test rig originates directly from the bearing as a result of under race lubrication. The film is also fed by the large droplets/ligaments, created during the interaction between the rolling element and the bearing cage, which are catapulted towards the bearing chamber outer wall [8]. From the film generation mechanisms it can be said that the film velocity is negligibly small as compared to the air velocity. As a result of air/oil interaction, a complex two-phase shearing flow dominates the bearing chamber. Based on the comprehensive investigations in the model bearing chamber, Gorse [8] summarized the two-phase flow phenomena which might be governing real engine bearing chambers (see Fig. 2)

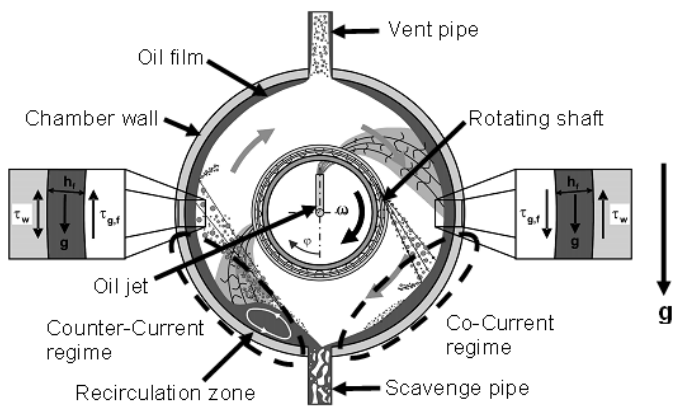


Figure 2. Two phase phenomena in model bearing chambers

In the past, the film flow in bearing chamber was treated as rimming flow. Hence it was assumed that shear is the major driving force and gravity has only a limited influence on the film dynamics even in the counter current regime. This however as depicted in Fig. 2, seems not to be the general case for some configurations even for shaft speeds as high as 12000 rpm [8]. Consequently all thin film models proposed in the past e.g. [7, 11, 12, 13] for predicting the film thickness distribution show only limited success. The partial flow reversal (recirculation zone) with local film thickening cannot be

reproduced by the thin film models due to fundamental model limitation. Therefore provisions are necessary to investigate the characteristics of the film in the counter current regime as well before the film can be modelled accurately. The superposition of several factors (e.g. droplet-film interaction, off-take disturbances etc), limitations on optical access and measurement technique makes it very difficult to investigate the individual characteristics of the film in the model bearing chamber test rigs. Moreover, any quantitative analysis of the film is usually very sensitive to the choice of boundary conditions which in 1:1 bearing chamber test rigs are very difficult to determine accurately. The growing interest in CFD technique also requires well defined boundary conditions and understanding of individual film characteristics before a superposition of all on the film dynamics (e.g. in bearing chambers) can be simulated. Therefore, test rigs reproducing bearing chamber typical wall flow with well defined boundary conditions are necessary, not only for analytical treatment but also to analyze the available multiphase models for wall film simulation. Accordingly a simple test rig was designed using similitude/similarity to the model bearing chamber test rig.

## NOMENCLATURE

<u>Symbols</u>	<u>Units</u>	<u>Physical Quantity</u>
$u$	[m/s]	Mean velocity
$g$	[m/s <sup>2</sup> ]	Acceleration due to gravity
$f$	-	Friction factor
$\dot{V}$	[l/min]	Film loading
$P_{T1}$	[Pa]	Total pressure in inlet module
$P_{S1}$	[Pa]	Static pressure in inlet module
$\Delta P$	[Pa]	Pressure drop in test section
$\Delta P_{Sr}$	[Pa]	Differential static pressure
$Fr$	-	Froude's number ( $u_L / \sqrt{g\delta}$ )
<u>Greek</u>		
$\rho$	[kg/m <sup>3</sup> ]	Density
$\delta$	[mm]	Film thickness
$\tau$	[Pa]	Shear stress
<u>Subscripts</u>		
$WF, WoF$	-	With liquid film, without liquid film
$G, L$	-	Gas, liquid
$S$	-	Superficial
$i$	-	Interface, interfacial
<u>Abbreviations</u>		
CFD	-	Computational fluid dynamics
ITS	-	Institut für Thermische Strömungs- maschinen
DOF	-	Degree of freedom

## EXPERIMENTAL SETUP

**Test rig design:** A model is said to have similitude with the real application if the two share geometric, kinematic and dynamic similarity. Geometric similarity is intentionally avoided based on the reasons stated earlier. Dynamic similarity is achieved by keeping the interface shear stress and the film thickness in the simplified test rig, similar to the observation made in the ITS model bearing chamber test rig. Similar interface shear stress is achieved by blowing the bearing chamber relevant air velocities on the liquid film with minimum possible initial film momentum for the relevant film thicknesses. The upper limit on the superficial gas velocity is restricted by the onset of liquid entrainment in the gas phase (droplet shedding).

A combination of the design of the pre-filming device, test rig dimensions and the film loading keep the film thickness similar to the near scavenge bearing chamber film thickness (3 - 5 mm) [1, 2, 4, 7]. The similar film thickness and the rotational DOF of the test rig assure similarity in film surface structure and gravitational force. The similar film surface structure implies that the air experiences similar surface roughness as in the bearing chamber environment. Kinematic similarity requires similar time rates of change of motions. Due to the fact that for the investigated flow phenomena dynamic similarity can be achieved to a satisfactory level, it is safe to assume that the kinematic similarity is also achieved.

A transparent modular test rig with a rectangular cross-section (192mm × 50mm) and a test section length of approximately 915 mm (see Fig. 3) was constructed. The large width of the test rig is to avoid considerable wall effects on the film flow. A uniform and homogenous liquid film is achieved by means of a compact pre-filming device designed in an iterative CFD procedure. The rig has a rotational degree of freedom

of up to 45° to analyse cases under pure gravitational effects as well as combined gravitational and shear effects. This way the test rig allows an effective isolation of the driving force, hence the influence of only the isolated force on the film dynamics can be studied. For effectively quantifying the influence of driving force, a new integral approach is used which gives the complete momentum transfer to the film. This approach is very effective in the sense that it gives a single measurable parameter characterising the complete flow field. In table 1 the investigated boundary conditions are listed. *Note: the reported film thickness is without gas flow and measured at the start of the test section. The reported superficial liquid velocity is with reference to the pre-filming device's constant entry section (192mm × 5mm).*

$u_{SG}$ [m/s]	$\dot{V}$ [l/min]	$\delta$ [mm]	$u_{SL}$ [m/s]
5 – 11	5.07	3	0.088
5 – 11	8.34	5	0.145

**Table 1. Investigated boundary conditions**

Air and water at room temperature and pressure are used as working fluids. For the shear driven wall films, interfacial shear stress, given by the relationship  $\tau_i = 0.5 f_i \rho_G (u_{SG} - u_{SL})^2$ , is the only mean of interaction between phases. Since the air density is a function

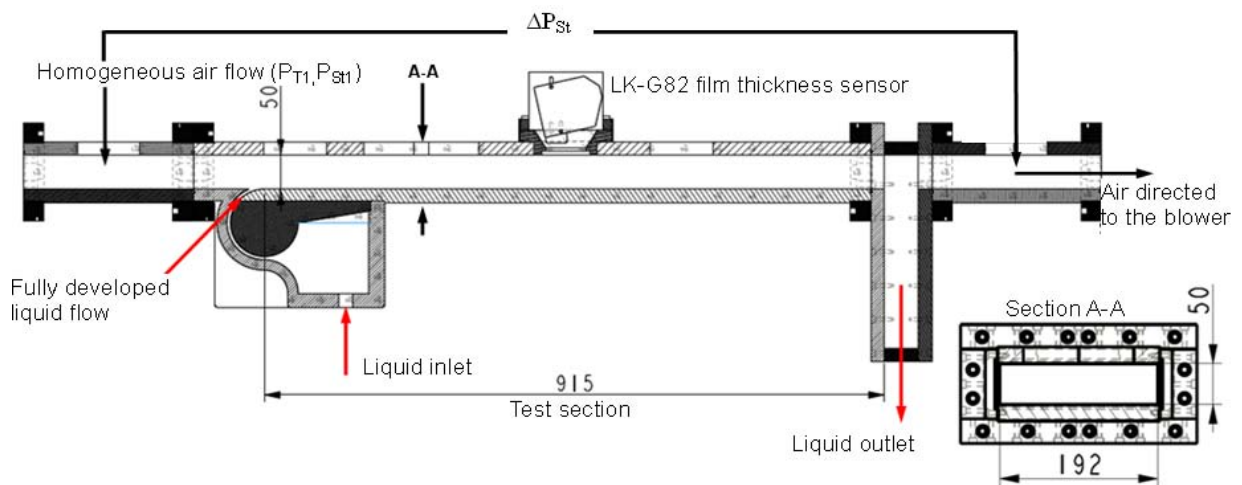


**Figure 3. Schematics of ITS stratified flow test rig**

of pressure therefore its affect does not need to be investigated explicitly. However care should be taken when transferring the results to high pressure systems because it can be shown that for an increase in density by a factor e.g.  $\rho = \alpha\rho_G$ , the upper limit (droplet shedding) on the superficial air velocity decreases by approx.  $u_{SG}/\sqrt{\alpha}$ . Water is chosen because the viscosity and density of water at room temperature are similar to those of aero-engine oil at typical operating temperatures of 100 - 200°C.

**Flow loop & instrumentation:** A blower of type RD 5 (19 m<sup>3</sup>/s, 50Hz) of the company Elektror is used to suck the air through the test rig. Air enters the inlet module from the undisturbed surrounding through a bell-shaped intake. The junction between the bell-shaped intake and the inlet module is further provided with a fine grid which generates a homogenously mixed block profile air flow. The total and static pressure of the air flow was measured, averaged over at least 30 seconds, with the help of a pitot tube connected to a MP 200 M (range  $\pm 2500$ Pa within  $\pm 2$ Pa) type manometer of the company KIMO<sup>®</sup> INSTRUMENTS. The derived dynamic pressure was used to determine the superficial air velocity and air flow rate at the inlet.

A 200 litre water reservoir, placed approx. 2.5 m above the test rig, supplies the required constant volume flow rate. The water flows in a closed loop and suitable measures are taken to keep a constant water level in the reservoir. This together with the pre-filming device allows for uninterrupted constant volume flow rate hence constant initial film conditions in the test rig. The supply pipe is provided with a G2 (range 3.8-37.9 litre/min within  $\pm 1.5\%$ ) turbine volume flow meter of the GPI<sup>®</sup> Industrial grade electronic digital meters. A digital computer attached to the instrument displays the instantaneous flow rate of the passing liquid.

Air interacts with the liquid film only in the test section. After the test section, the liquid is collected in the separator tank which is always filled with some liquid. The collector tank is continuously drained out at the same rate as the water enters the test section. This helps in achieving a constant liquid level in the tank and also keeps the complete air flow towards the outlet module with minimal disturbances. A simultaneous differential static pressure measurement, averaged over at least 30 seconds, between the inlet and the outlet module is also taken using the manometer of type MP 200 P (range  $\pm 500$ Pa within  $\pm 0.8$ Pa). The pressure drop in the test section is equal to the differential static pressure because the dynamic pressure (integrated over the cross-section) is constant in the inlet and outlet section (same cross-section and air volume flow rate). Therefore, it follows:

$$\Delta P \approx \Delta P_{St}$$

The measurement was repeated with and without film in the test section. The additional pressure drop gives the

complete momentum transferred to the film from the shearing air flow as follows:

$$\text{Momentum transfer to film} = \Delta P_{WF} - \Delta P_{WoF}$$

Contrary to the local film thickness measurement which can only be measured at a point or few, the momentum transfer is a global parameter yet very easy to determine. A comprehensive quantitative analysis can now be performed efficiently and effectively using this new parameter.

## RESULTS AND DISCUSSION

Every data point is repeated to ensure reproducibility. The point scatter reported in the figure 4 is achieved by keeping the liquid flow rate constant and setting a gas flow rate which is then reached by decreasing higher gas flow rates and by increasing lower gas flow rates. The gas flow rate is then kept constant and the liquid loading is varied. The reproducibility test during the experimental study can be summarized as follow:

- Varying gas flow rate and keeping the liquid flow rate constant leads to reproducibility within small tolerance of  $\pm 2$  Pa. This deviation results from system hysteresis
- Varying liquid flow rate and keeping the air flow constant leads to high reproducibility

A good reproducibility indicates that the introduced technique is generally valid for analyzing undeveloped multiphase flows of discussed nature.

**Co-Current flow regime:** In this flow regime, the driving forces are acting in the same direction (see figure 2). The horizontal co-current flow regime is of little importance for the bearing chamber; however it can be used to effectively appreciate the influence of gravitational force on the thick wall films.

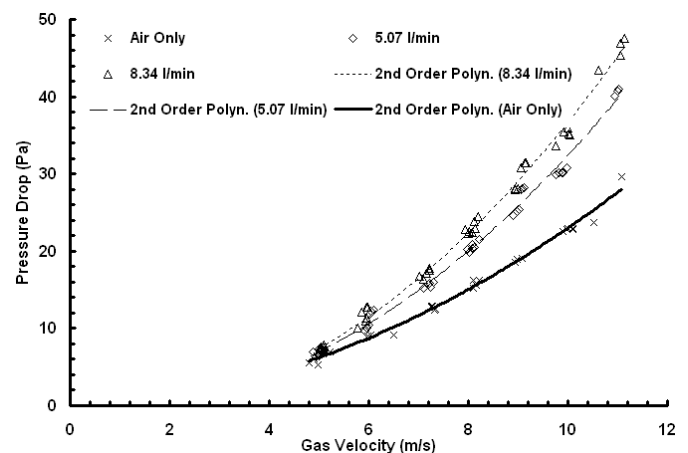


Figure 4. Influence of film loading on pressure drop

The pressure drops measured in the gas flow without (Air Only) and with liquid loading (5.04, 8.34l/min) are plotted

against the increasing gas velocity in Fig. 4. The curves are 2<sup>nd</sup> degree polynomial fit ( $R^2 > 0.99$ ) of the measured data points. The choice of a second order polynomial is based on the physical reason that the pressure loss in a turbulent flow is proportional to the square of the mean flow velocity. This behaviour remains true in the presence of liquid film in the test section suggesting that the air flow experiences the liquid film as an additional resistance leading to additional pressure loss.

For the qualitative analysis, a number of pictures characterising the film surface instabilities are taken. The recorded area is shown by the bold rectangle in Fig. 5.

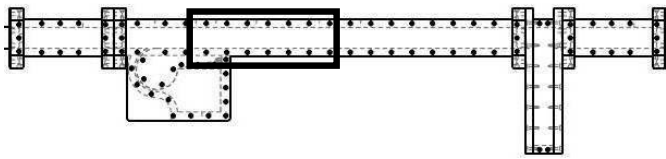


Figure 5. Photographed window for co-current analysis

In the following figures (fig.6a-b), a series of pictures with increasing gas velocity for the two investigated film loadings are shown. Figure 6a corresponds to the 5.07 l/min film loading and an initial film thickness of 3mm. Similarly, figure 6b corresponds to the 8.34 l/min film loading and an initial film thickness of 5 mm in the test section.

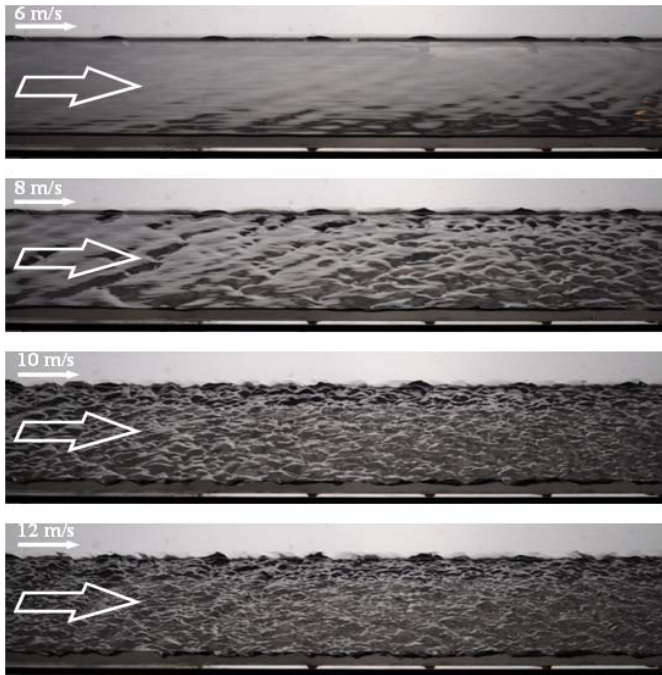


Figure 6a. Co-Current waveforms in horizontal case (5.07 l/min)

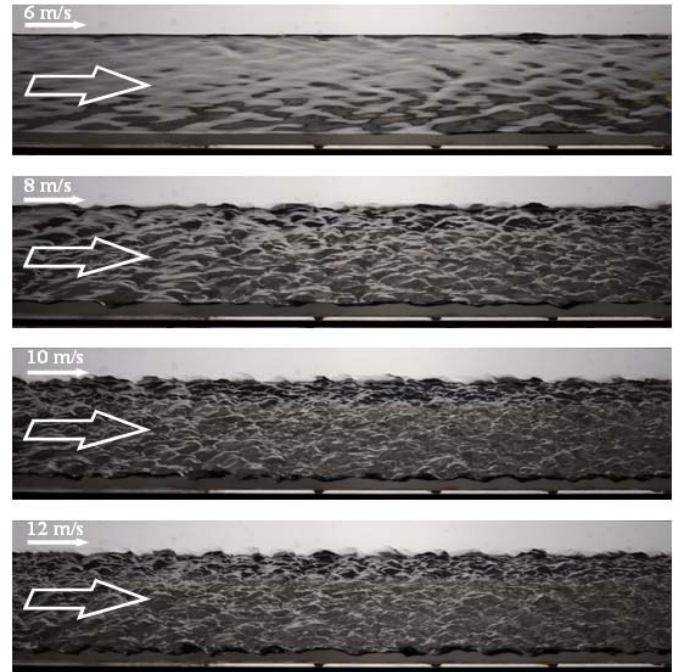


Figure 6b. Co-Current waveforms in horizontal case (8.34 l/min)

The Figures 6a-b show that increasing the gas velocity results in similar waveforms for the low as well as high film loading. The difference lies only in the wave amplitude which is relatively bigger, due to higher momentum transfer, for high film loading at the same gas velocity. This can be explained by taking into account that higher film loading results in thicker film hence the gas flow path is reduced. For the same superficial gas velocity, reduced flow path means higher local velocity in the test section hence higher interface shear stress. Fig. 4 also confirms this behavior where high film loading incurs higher pressure losses than the low film loading case.

The behavior of the gas-liquid interface as presented in the figures can be described as follows. The first transition from the flat/smooth gas-liquid interface to the inception of small surface instabilities begins at a gas velocity of 6 m/s. As the gas velocity was increased, it was observed that a 3D wave occupying the entire channel width appeared (see 2<sup>nd</sup> picture from top in fig. 6a) which after a certain entrance length divides and multiplies into a number of 3D waves. This happened around 7-8 m/s gas velocity. With increasing shear on the film surface, the amplitude and frequency of the 3D waves increases with a decrease in entrance length. Further increase in the gas velocity at times resulted in droplets tearing-off from the wave peaks. This point usually occurred beyond a gas velocity of 12 m/s and therefore not dealt within the scope of this paper.

As mentioned earlier, to simulate the bearing chamber typical wall film flows gravitational effects must be included (see Fig. 2). Therefore, the investigations carried out in the

horizontal test rig configuration were complemented with tests inclining the rig up to 25° in the interval of 5° (figure 7a-b). From 15° onwards no considerable difference could be recorded in the measured parameter (momentum transfer), therefore larger than 25° inclination angles were not investigated.

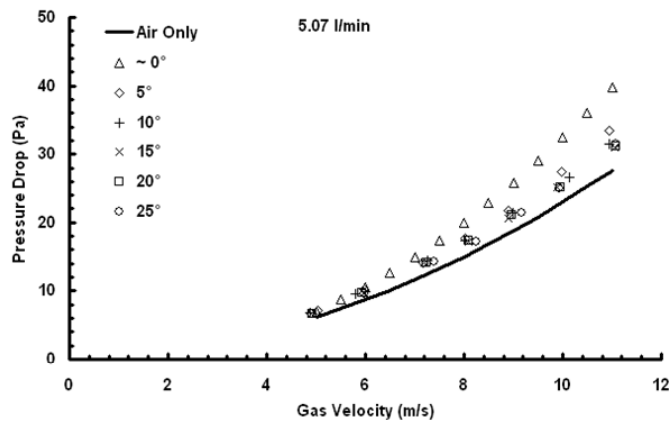


Figure 7a. Influence of inclination on pressure drop (5.07 l/min)

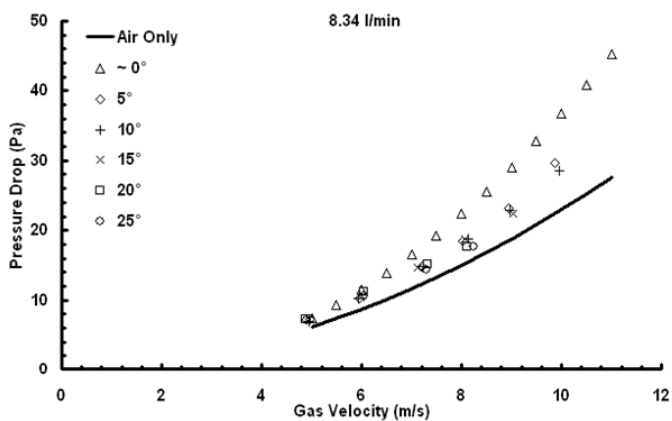


Figure 7b. Influence of inclination on pressure drop (8.34 l/min)

The plots indicate that for thick films, even a small inclination angle of 5° has a noticeable effect on the pressure drop measurements (see ~ 0° in fig. 7 a-b). With increasing inclination angle the pressure drop continuously decreases. From 15° onwards, no further change in the pressure drop could be recorded and the distributions almost overlapped. This behaviour remains even with increasing the gas velocity. The lack of data for higher inclination angle and gas velocity is due to the fact that the liquid film starts to jump (due to gravity induced additional momentum) over the separator tank hence further measurements could not be taken. The behaviour of the

film however remains consistent, therefore the curves can be extrapolated as long as the film remains sub-critical (no droplet shedding).

For the qualitative analysis pictures corresponding to the same pattern as shown in Fig. 5 are provided (see Fig. 8). Since different film loadings did not show considerable differences, only the pictures corresponding to the 5.07 l/min film loading are presented. Furthermore, the film surface deforms only slightly in the inclined case, therefore only pictures corresponding to the highest investigated superficial gas velocity (~12 m/s) are shown to demonstrate the strong influence of gravitational force on thick films.

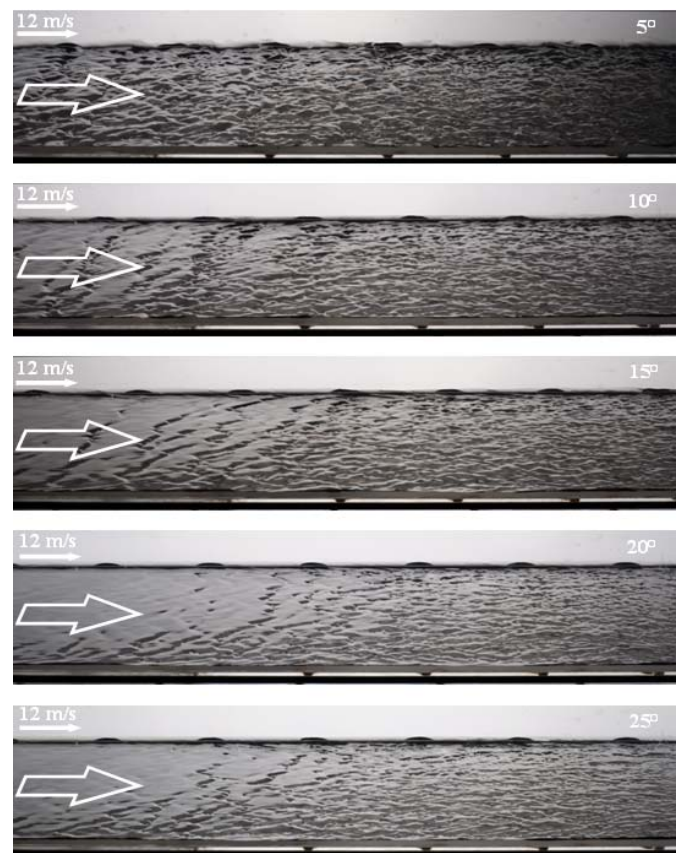


Figure 8. Co-Current waveforms in inclined case ( $u_{GS} = 12\text{m/s}$ )

It can be observed that increasing the inclination results in a decrease in wave amplitude and frequency i.e. increase in wave length. When compared to the corresponding horizontal configuration where 12 m/s can be seen as the droplet shedding limit, the film remains very stable with no sign of droplet shedding. The wave generation mechanism however remains consistent with the horizontal case i.e. a single 3D wave which spreads along the width, distorts and divides into a number of smaller waves (see 2<sup>nd</sup> picture from top in fig. 8). The entrance length increases with

inclination angle because the film accelerates, which results in the decreased interface shear stress. From 15° onwards the film surface structure can be regarded as constant (see Fig. 8). This behaviour can now be traced back to the quantitative analysis (Fig. 7a-b) where from 15° onwards the pressure drop curves start to overlap. The pressure drop depends on the flow cross-sectional area and the surface roughness, therefore it can be said that the film dynamics which constitute of film thickness and film surface roughness (due to interface waves) remains constant. From 15° onwards, the constant film dynamics hypothesis can only be explained by assuming fully developed conditions. This can be proved theoretically by considering only the film flow (without interface shear) in the test section. A continuous increase in the inclination angle imparts an additional momentum to the film, which according to  $\rho_L g \delta \sin \theta$  is governed by the film thickness and the gravitational force. For a constant film loading, the film experiences a continuous decrease in the thickness with the corresponding increase in velocity. At a critical inclination angle the film thickness decreases to a point where the viscous force becomes equal to the gravitational force i.e. a transition from thick to thin film occurs. The film can now also be considered as both laminar and fully developed in the test section. The measured film thickness (5.07 l/min ~1.5 mm, 8.34 l/min ~2 mm) also indicates that the gravitational force drives the film to supercritical regime ( $Fr > 1$ ). Returning to the original problem of sheared film flows, it can be stated that the flow phenomena explained above is only enhanced by the fast moving gas flow above the film surface.

**Counter-Current flow regime:** In this flow regime, the driving forces act in the opposite direction (see Fig. 2). All counter-current pressure drop measurements are achieved with the help of a ramp arrangement, shown by a bold black line in the Fig. 9, in the outlet module. The sharp edge junction between the test section and the separator tank, shown by a light grey filled circle in the Fig. 9, leads to film roll ups and premature droplet shedding. The ramp arrangement was used to assist a smooth gas liquid interaction in the test section.

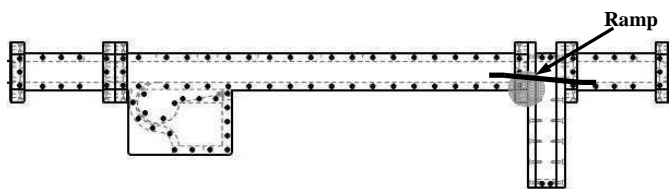


Figure 9. Ramp arrangement for counter-current measurements

In Fig. 10a-b, the influence of film loading on pressure drop is studied with the help of two (5° & 25°) inclination angles. Up to a certain air velocity, the film behaves in the similar manner as under pure gravity and no additional pressure drop could be measured. Beyond this air velocity a

transition both in pressure drop and film behavior takes place. The increase in film loading results in a shift of transition point to slightly lower gas velocity for all inclination angles. This is due to fact that relatively thicker film results in higher local gas velocity hence higher interface shear stress. This, as will be shown later, results in early inception of surface instabilities and expected higher pressure drop. This behaviour is more obvious for 5° than for 25° inclination. For large inclination angles this is not the case because constant film dynamic governs the flow. Hence from the critical angle of 15°, the transition points for different film loadings lay close to each other (see Fig.11a-b). The curves however, exhibit different slopes due to different film momentum that has to be overcome by the counter acting air flow.

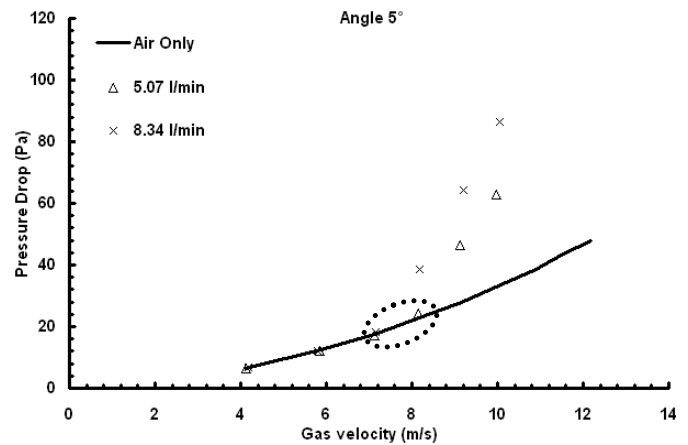


Figure 10a. Influence of film loading on pressure drop (5°)

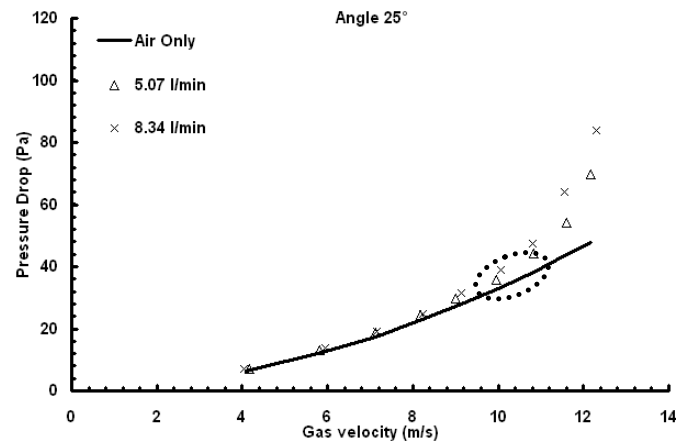


Figure 10b. Influence of film loading on pressure drop (25°)

Increasing the inclination angle with constant film loading is investigated in the Figures 11a-b. The transition point shifts towards higher air velocity in both the investigated film loadings. This behavior is quite plausible because the counter-current air flow has to overcome the gravity induced additional momentum. An interesting fact to be noted here is

that although the transition point shifts towards higher air velocity for larger inclination angles, the pressure drop incurred at lower angle for the same air velocity is much higher. As an example compare the curves of 5° & 25° inclination angles in figures 11a-b at 10 m/s air velocity. The high pressure drop incurred at 5° inclination as compared to the 25° is attributed to the early transition from flat to wavy surface. The waves then grow with increasing air velocity, as will be discussed later in the qualitative analysis, hence higher pressure drops. From 15° onwards, the transition point lies again very close to each other but the slope decreases with increasing inclination angle i.e. for a constant film loading, increasing inclination angle means that the film incurs smaller pressure losses. From the principle of constant film dynamics, the film thickness hence film velocity remains constant. On the other hand increasing inclination angle allows only smaller wave amplitudes due to higher gravitational influence (as will be discussed in the next section). Therefore, the film surface roughness reduces and results in a smaller pressure drop for the same conditions.

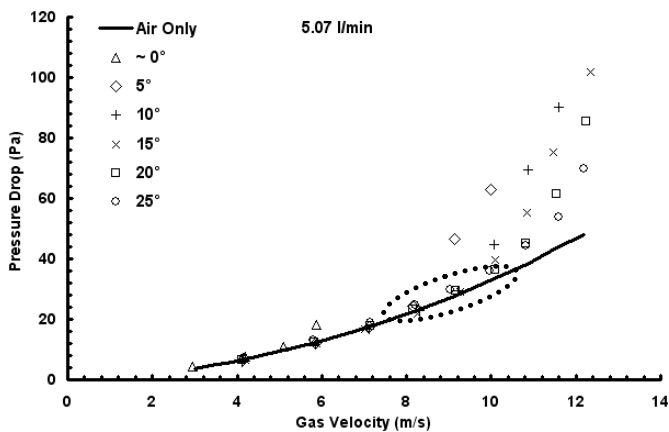


Figure 11a. Influence of inclination on pressure drop (5.07 l/min)

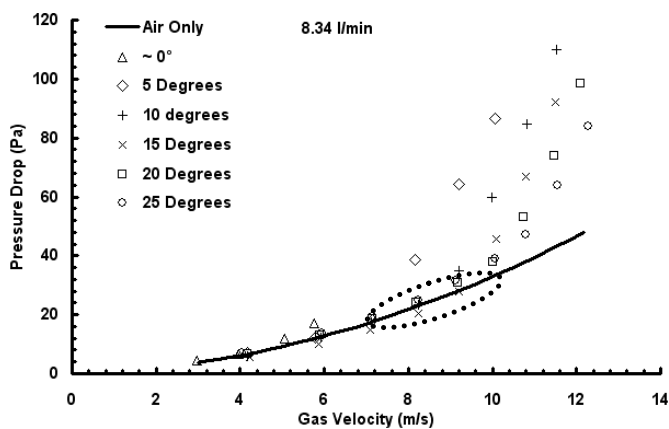


Figure 11b. Influence of inclination on pressure drop (8.34 l/min)

A qualitative analysis corresponding to the quantitative analysis is done in the following section. The recorded window in the pictures is identified by the bold rectangle in the Figure 12.

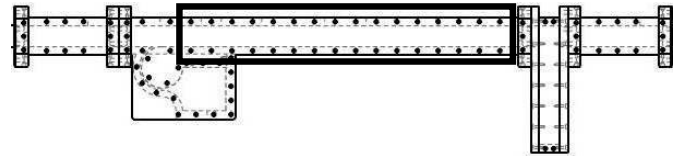


Figure 12. Photographed window for counter-current analysis

Unlike co-current flow, in counter-current flow not all waveforms were present for all boundary conditions. Up to 5° inclination angle the observed waveforms could be classified into three (see Fig. 13a) whereas from 10° onwards only the last two waveforms could be observed (Fig. 13b).

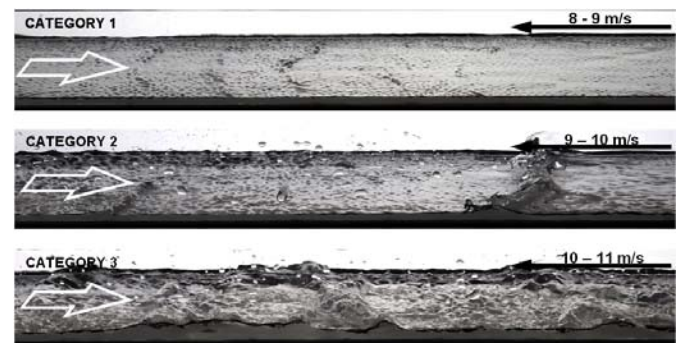


Figure 13a. Counter-Current waveforms up to 5°

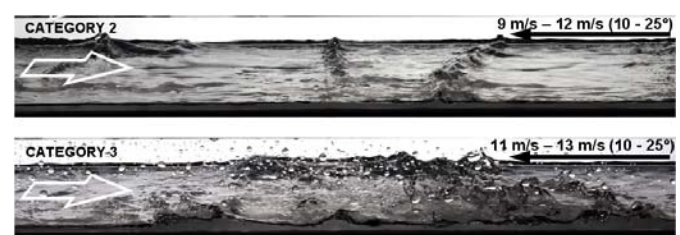


Figure 13b. Counter-Current waveforms from 10° onwards

With reference to the Figure 13a, *Category 1* type waves constitute of very small ripple like surface disturbances lacking any considerable motion. From 10° onwards, this waveform could not be observed. This could be seen as a direct influence of gravitational force i.e. the film is accelerated to an extent that the air velocity needed to produce such surface ripples is high enough to directly trigger the next wave regime, as will be evident in the following. *Category 2* waves consist of

periodic solitary waves (usually two waves along the channel length) which were seen to occupy the complete channel's width with wave tip pointing in the direction of gravity vector. This is due to the fact that the air flow is not strong enough to carry the thick wave along the channel length resulting in a recirculation zone on the film surface. The solitary waves were 0.3 – 0.4 m apart and display to-and-fro motion (travelled couple of centimetres downstream then returned to the same position) on the film surface. Between the solitary waves the film surface was only occupied by small disturbances. Occasional droplet shedding from the tip of the solitary wave was also observed. From 10° onwards the same waveform was observed but with smaller amplitude and the surface between the solitary waves was almost flat (Fig. 13b). Large gravitational influence on the film dynamic, as explained earlier, is responsible for this behaviour. In *Category 3*, the solitary waves of *Category 2* became non-uniformly distributed along the channel width with much higher frequency than the *Category 2* solitary waves. To-and-fro motion stops and the waves begin to travel downstream along the channel length. The film surface between the consecutive solitary waves was reduced to 0.1 – 0.2 cm and was occupied by variable amplitude 3D waves. Low rate continuous droplet shedding was also observed in this category. From 10° onwards, the same waveforms could be observed but with relatively small amplitude for the same reason as mentioned above. In general, it can be stated that the counter-current flow regime after the formation of *Category 2* type waveform, is always susceptible to droplet shedding from the wave tips.

## CONCLUSIONS

From the investigations carried out in this paper, some simple rules for the momentum transfer to film and transition from flat to wavy film surface in co- as well as counter-current flow regime can be given. For thicker films momentum transfer is higher and transition is earlier than for thinner films where comparatively lower momentum transfer and late transition was observed.

Applying the findings to bearing chamber flows, this investigation reveals that the sealing air experiences almost no resistance on the co-current side. Furthermore, the oil film on the co-current side, as discussed earlier can be categorized as laminar/nearly laminar and supercritical. The experiments conducted by Glahn et al. (1996) [3] in the ITS model bearing chamber test rig also confirm these finding where none of the measured (film) velocity profile could be found as fully turbulent. Moreover, increasing interface shear shows a clear tendency towards laminar velocity profile. The Froude number calculated from the film velocity profile data by Glahn (1996) et al. [3] also shows that the film was super-critical for all boundary conditions. Another significance of this investigation is that the film dynamics in the horizontal case are not representative for inclined cases. After a critical inclination angle, a transition from thick to thin (*viscous force*  $\approx$  *gravitational force*) film can be

theoretically proved. Accordingly, the film surface waves are largely damped in the inclined configuration. The roll waves usually responsible for the droplet generation from the thin films however require much higher air velocity to appear on thin [14] than on thick films. Therefore it can be said that for the maximum possible mean air velocity [2] experienced by the film in the ITS model bearing chamber, the droplet generation is very unlikely from the co-current side.

On the other hand, the sealing air flow sees major resistance on the counter-current half of the bearing chamber. High air velocities always result in solitary waves for all inclination angles. Considering the ITS model bearing chamber test rig (see Fig. 1), where according to Glahn (1995) [2] a mean velocity of approx. 15 m/s and 10 m/s (while simulating the high and intermediate pressure bearing chamber) can be calculated, it can be predicted that *Category 3* type waves dominates the counter-current side in case of high and *Category 2* type waves dominate the intermediate pressure bearing chamber. In addition to that, the nature of droplet shedding i.e. either low rate continuous or occasional from the wave tips can also be predicted. After the transition point, the film can be considered as turbulent and sub-critical. The film is regarded as turbulent according to the general definition of turbulent flow i.e. transverse exchange of momentum, in other words high mixing in the recirculation region formed by solitary waves. From the experiments conducted using the ITS model bearing chamber test rig e.g. [4, 8], indeed an unstable recirculation region with droplet shedding and high mixing was identified on the counter-current side. The sub-critical nature of the film can be defended on the basis of continuous reduction in mean velocity and continuous increase in film thickness. Gargallo et al. (2005) [9] and Stähler et al. (2006) [10] have explained this super to sub-critical transition before partial flow reversal occurs on the film surface (in the direction of counter air flow) in more detail.

Regarding losses in bearing chambers, from the pressure drop curves it can be said that the oil film incurs minimal losses on the co-current side. After the transition point, the counter-current flow regime always incurs higher pressure losses for all boundary conditions. For the counter-current regime, further increase in the air velocity beyond the investigated range will soon results in complete flow reversal accompanied with high rate of droplet shedding. However, a clean rimming (film) flow as explained earlier is very unlikely. Furthermore on the basis of huge difference in momentum transfer, the assumption of rimming flow for analytical models is ambiguous. As can be seen from the Figures 14a-b, the sealing air losses approx. 10 order of magnitude more energy in the counter-current regime than in the co-current regime. This is due to the fact that in the counter-current regime sealing air works against the gravity whereas in co-current regime gravity assists the shearing air flow. From the discussions, it is also apparent that the churning losses in bearing chamber as a result of air/oil interaction must also be much larger on the counter-current side than on the co-current side.

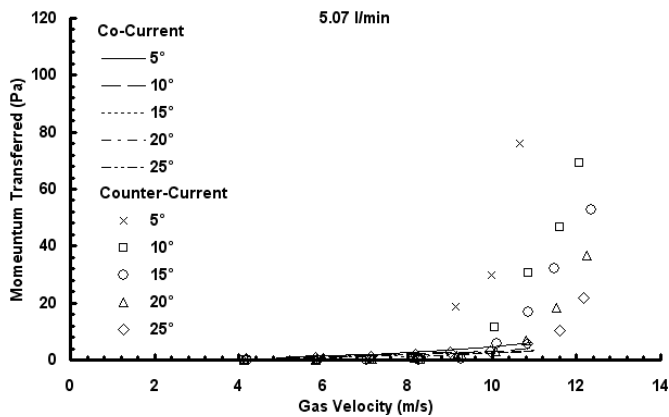


Figure 14a. Co/Counter-Current momentum transfer (5.07 l/min)

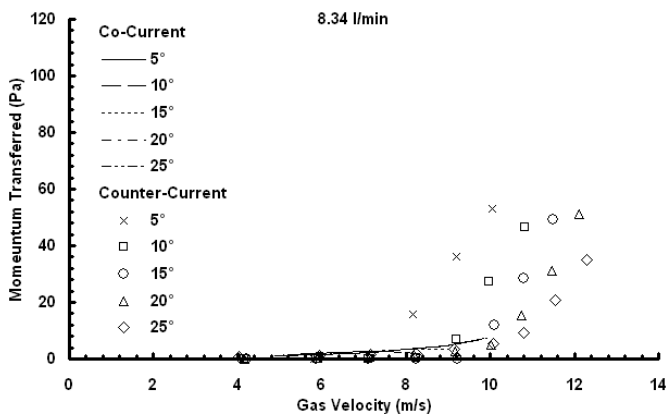


Figure 14b. Co/Counter-Current momentum transfer (8.34 l/min)

The major difference between the investigations presented here to most of the prior published studies is that a global quantitative analysis of the film was conducted with the help of a parameter determined from the single phase measurements (only in air). Hence the film dynamics were not studied directly but by considering how the air experiences the film. If the film was analyzed directly, only local quantities like film thickness/velocity profile could be measured at a point or few, which is not sufficient for describing the behaviors of complicated (3D) and undeveloped sheared film flows. Another benefit is, since only air was measured to determine the momentum transferred to the film, the data provided here depends only on the air properties. Therefore, the parameter introduced here and information about its trends will be useful with other film properties too. Due to the possibility of different film surface structure (waves) which can arise from different film properties an offset may result, nevertheless the physics explained here will remain. It can also be argued that the data trends provided here are equally valid for oil film

properties relevant to the bearing chamber. Typically, oil film in bearing chamber has smaller surface tension and higher viscosity than water. From the open literature [15, 16] it can be stated that the reduced surface tension and higher viscosity result in a dampening effect on the surface waves and delay in droplet shedding compared to water.

## SUMMARY

ITS (model) bearing chamber test rig revealed that the thick (near scavenge) oil film may behave differently in the co- & counter-current regime even for very high shaft speeds (no simple rimming flow). From the similarity principle, a simple test rig capable of simulating bearing chamber typical oil film in the co- & counter-current regime was designed. The test rig offers well-defined boundary conditions and employs an effective yet very easy to measure parameter for the quantitative analysis of the undeveloped oil film. The complete (integral) energy/momentum transferred to the film from the shearing air flow can be measured using the introduced parameter. It was found that the air experiences the oil film in both regimes as an additional resistance (in the test section); consequently the losses were proportional to the square of the mean air superficial velocity. With the help of qualitative analysis, the waveforms in the co-/counter-current flow regime are categorized. The qualitative analysis also indicates that the droplets in bearing chambers are most probably generated from the counter-current side. From the quantitative and qualitative analysis conducted in this paper, some plausible characteristics of the oil film dynamics near the scavenge off-take (in the absence of coexisting flow phenomena e.g. droplet interaction, off-take disturbance etc...) can be summarized, which are as follows:

Co-Current	Counter-Current
<ul style="list-style-type: none"> <li>▪ Flat surface or shallow waves</li> <li>▪ Very low probability of droplet shedding</li> <li>▪ Laminar/nearly laminar</li> <li>▪ Supercritical</li> <li>▪ Can be considered as fully developed</li> <li>▪ Almost no churning loss</li> </ul>	<ul style="list-style-type: none"> <li>▪ Big solitary waves</li> <li>▪ Droplet shedding</li> <li>▪ Turbulent</li> <li>▪ Sub-critical</li> <li>▪ Definitely undeveloped</li> <li>▪ Large churning losses</li> </ul>

## ACKNOWLEDGMENTS

The financial support from the German Federal Ministry of Economics and Technology and Rolls-Royce Deutschland within the cooperative research project 'Luftfahrtforschungsprogramm 2007-2010 (LuFo-20T0605)' is

highly appreciated. The author would also like to thank Dr. Rainer Koch for sharing his experience on multiphase experimental techniques.

## REFERENCES

- [1] Wittig, S., Glahn, A. and Himmelsbach, J., 1994, "Influence of High Rotational Speeds on Heat Transfer and Oil Film Thickness in Aero Engine Bearing Chambers", ASME Journal of Engineering for Gas Turbines and Power, 116, pp. 395–401.
- [2] Glahn, J.A., 1995, "Zweiphasenströmungen in Triebwerkslagerkammern - Charakterisierung der Ölfilmströmung und des Wärmeübergangs", Dissertation, Institut für Thermische Strömungsmaschinen, Karlsruher Institut für Technologie (KIT)
- [3] Glahn, A. and Wittig, S., 1996, "Two-Phase Air/Oil Flow in Aero Engine Bearing Chambers: Characterization of Oil Film Flow", ASME Journal of Engineering for Gas Turbines and Power, 118(3), pp. 578–583.
- [4] Schmälzle, C., 1997, "Charakterisierung der Ölfilmströmung in Triebwerkslagerkammern - Strömungsvisualisierung und Filmgeschwindigkeitsmessungen mit Hilfe der Laser Doppler Anemometer". Studienarbeit, Institut für Thermische Strömungsmaschinen, Karlsruher Institut für Technologie (KIT)
- [5] Busam, S., Glahn, A. and Wittig, S. (2000): Internal Bearing Chamber Wall Heat Transfer as a function of Operating Conditions and Chamber Geometry. ASME, Journal of Engineering for Gas Turbines and Power, 116, S. pp. 395–401.
- [6] Schober, P., 1998, "Bewertung unterschiedlicher Gestaltungskonzepte am Eintritt von Abluft und Absaugleitungen in Lagerkammern". Diplomarbeit, Institut für Thermische Strömungsmaschinen, Karlsruher Institut für Technologie (KIT)
- [7] Gorse, P., Busam, S. & Dullenkopf, K., 2004, "Influence of Operating Condition and Geometry on the Oil Film Thickness in Aero-Engine Bearing Chambers", ASME Journal of Engineering for Gas Turbines and Power, 128(1), pp. 103-110
- [8] Gorse, P., 2006, "Tropfenentstehung und Impulsaustausch in Lagerkammern von Flugtriebwerken", Dissertation, Institut für Thermische Strömungsmaschinen, Karlsruher Institut für Technologie (KIT)
- [9] Gargallo, M., Schulenberg, T., Mayer, L., Laurien, L., 2005. Counter-current flow limitations during hot leg injection in pressurized water reactors. Nucl. Eng. Des. 235, 785–804
- [10] Wintterle, T., Laurien, E., Stäbler, T., Meyer, L., Schulenberg, T., 2006, "Experimental and Numerical Investigation of Counter-current Stratified Flows in Horizontal Channels". Nucl. Eng. Des. 238, pp. 627–636
- [11] Chew, J.W., 1996, "Analysis of the Oil Film on the Inside Surface of an Aero Engine Bearing Chamber Housing", ASME Paper No. 96-GT-300.
- [12] Farrall, M., Hibberd, S., Simmons, K., Busam, S., Gorse, P. and Dullenkopf, K., 2004, "A Numerical Model for Oil Film Flow in an Aero-Engine Bearing Chamber and Comparison with Experimental Data", ASME-Paper GT2004- 53698.
- [13] Shimo, M., Canino, J.V., and Heister, S.D., 2005, "Modeling Oil Flows on Seal Runners and Engine Sump Walls", ASME Journal of Engineering for Gas Turbines and Power, 127(4), pp. 827-835
- [14] Cohen, L. S. and Hanratty, T. J., 1965, "Generation of waves in the concurrent flow of air and a liquid", AIChE 11, pp. 138-144
- [15] Hanratty, T.J. & Hershman, A., 1961, "Initiation of Roll Waves", A.I.Ch.E. Journal, 7(3), pp. 488-497
- [16] Weissman, J., Duncan, D., Gibson, J. & Crawford, T., 1979, "Effects of Fluid Properties and Pipe Diameter on Two-Phase Patterns in Horizontal Lines", International Journal of Multiphase Flow, Vol. 5, pp. 437-462